

# Application of the first collision source method to CSNS target station shielding calculation<sup>\*</sup>

Ying Zheng(郑颖)<sup>1</sup> Bin Zhang(张斌)<sup>1</sup> Meng-Teng Chen(陈蒙腾)<sup>1</sup>  
 Liang Zhang(张亮)<sup>1</sup> Bo Cao(曹博)<sup>1</sup> Yi-Xue Chen(陈义学)<sup>1;1)</sup> Wen Yin(殷雯)<sup>2</sup>  
 Tian-Jiao Liang(梁天骄)<sup>2</sup>

<sup>1</sup>School of Nuclear Science and Engineering, North China Electric Power University, Beijing 102206, China

<sup>2</sup>Institute of Physics, Chinese Academy of Sciences, Beijing 100190, China

**Abstract:** Ray effects are an inherent problem of the discrete ordinates method. RAY3D, a functional module of ARES, which is a discrete ordinates code system, employs a semi-analytic first collision source method to mitigate ray effects. This method decomposes the flux into uncollided and collided components, and then calculates them with an analytical method and discrete ordinates method respectively. In this article, RAY3D is validated by the Kobayashi benchmarks and applied to the neutron beamline shielding problem of China Spallation Neutron Source (CSNS) target station. The numerical results of the Kobayashi benchmarks indicate that the solutions of DONTRAN3D with RAY3D agree well with the Monte Carlo solutions. The dose rate at the end of the neutron beamline is less than 10.83  $\mu\text{Sv/h}$  in the CSNS target station neutron beamline shutter model. RAY3D can effectively mitigate the ray effects and obtain relatively reasonable results.

**Keywords:** CSNS, ARES, RAY3D, discrete ordinates method, first collision source method

**PACS:** 28.20.Gd, 28.41.Ak **DOI:** 10.1088/1674-1137/40/4/046201

## 1 Introduction

The discrete ordinates method is the most widely used deterministic method to obtain numerical solutions of the linear Boltzmann equation and to evaluate the dose rates in nuclear devices. However, this method suffers from an inherent problem, which is called the “ray effect”. The ray effects always cause a large distortion in the calculation results. The increasing of quadrature order can mitigate the ray effects, but the increase in calculation time is unacceptable. Hence, to improve the accuracy and efficiency of the discrete ordinates code system, development of a ray effect elimination module is of vital importance.

The China Spallation Neutron Source (CSNS) is under construction in Dongguan, China, and it will be the first Spallation Neutron Source facility in a developing country. The neutron beamline shutter [1] is a critical piece of equipment in the CSNS target station. To guarantee personnel security, shielding calculation for this shielding design is crucial. However, when using the discrete ordinates method to simulate this kind of deep

penetration problem with a channel of up to 10 m, the results always show unacceptable error because of the ray effects. In this paper, we calculate and analyze the practical neutron beamline shutter problem using the ARES code system. In the ARES code system [2], RAY3D employs the first collision source method [3] to mitigate the ray effects. RAY3D is validated by the Kobayashi benchmarks [4] and applied to the China Spallation Neutron Source target station neutron beamline shutter engineering problem.

Results obtained by the ARES module DONTRAN3D with RAY3D, DONTRAN3D and TORT are presented.

This paper is organized as follows. Section 2 briefly discusses the ARES code system and states the first collision source theory in detail. Section 3 validates the accuracy of RAY3D by using Kobayashi benchmarks. In Section 4, we introduce the CSNS target station neutron beamline shutter model and the main calculation parameters. Section 5 analyzes the results, and Section 6 concludes this article.

Received 3 June 2015

<sup>\*</sup> Supported by Major National S&T Specific Program of Large Advanced Pressurized Water Reactor Nuclear Power Plant (2011ZX06004-007), National Natural Science Foundation of China (11505059, 11575061), and the Fundamental Research Funds for the Central Universities (13QN34).

1) E-mail: yxchen1972@126.com

©2016 Chinese Physical Society and the Institute of High Energy Physics of the Chinese Academy of Sciences and the Institute of Modern Physics of the Chinese Academy of Sciences and IOP Publishing Ltd

## 2 RAY3D code

### 2.1 Introduction to ARES code system

The ARES code system, developed by the School of Nuclear Science and Engineering in North China Electric Power University, is a multi-group  $S_N$  particle transport code system with arbitrary order anisotropic scattering. It employs the discrete ordinates method to calculate and analyze the shielding efficiency of nuclear devices. ARES consists of Pre, DONTRAN, RAY and Post modules. Pre and Post are used to preprocess and reprocess the input and output information respectively. As the deterministic solver of ARES, DONTRAN calculates the flux distribution of models accurately. RAY eliminates the ray effects by the first collision source method. RAY3D is the 3-D ray effect elimination module of the ARES code system. So far, ARES has been verified by authoritative benchmark problems [5] and it has been applied to many complicated nuclear facilities.

### 2.2 RAY3D and the first collision source theory

RAY3D, a three-dimensional ray effect elimination code, employs the semi-analytic first collision source theory [3] to mitigate the ray effects. The ray effects, resulting from the limited number of discrete directions, are especially serious in systems which have a void region in a highly absorbing medium [5]. The ray effects always act on the space oscillation of flux distribution and cause enormous error in the results.

The first collision source method decomposes the flux into uncollided and collided components. The uncollided flux component is calculated analytically by RAY3D, and the collided flux component is calculated by DONTRAN3D.

The multigroup method is used for energy discretization in the transport equation:

$$\Omega \cdot \nabla \psi^g(r, \Omega) + \Sigma_t^g(r) \psi^g(r, \Omega) = S^g(r, \Omega). \quad (1)$$

The spherical harmonics expansions are applied to the scattering source term:

$$\begin{aligned} & \Omega \cdot \nabla \psi^g(r, \Omega) + \Sigma_t^g(r) \psi^g(r, \Omega) \\ &= \sum_{g'=0}^G \sum_{l=0}^N \frac{2l+1}{4\pi} \Sigma_{sl}^{gg'}(r) [Y_{l0}^e(\Omega) \phi_{l0}^{g'}(r) \\ &+ \sum_{m=1}^l (Y_{lm}^e(\Omega) \phi_{lm}^{g'}(r) + Y_{lm}^o(\Omega) \vartheta_{lm}^{g'}(r))] + q_e^g(r, \Omega), \quad (2) \end{aligned}$$

where the spherical harmonics moments of the angular flux of group  $g$  are defined by

$$\phi_{lm}^g(r) = \int_{4\pi} Y_{lm}^e(\Omega) \psi^g(r, \Omega) d\Omega, \quad m \geq 0, \quad (3)$$

$$\vartheta_{lm}^g(r) = \int_{4\pi} Y_{lm}^o(\Omega) \psi^g(r, \Omega) d\Omega, \quad m > 0, \quad (4)$$

$\phi^g$  are even order flux moments,  $\vartheta^g$  are odd order flux moments.

Here

$$\begin{aligned} & Y_{lm}^e(\theta, \varphi) x \\ &= (-1)^m \sqrt{(2-\delta_{m0}) \frac{2l+1}{4\pi} \frac{(l-m)!}{(l+m)!}} P_{lm}(\cos\theta) \cos m\varphi, \quad (5) \end{aligned}$$

$$Y_{lm}^o(\theta, \varphi) = (-1)^m \sqrt{\frac{2l+1}{2\pi} \frac{(l-m)!}{(l+m)!}} P_{lm}(\cos\theta) \sin m\varphi, \quad (6)$$

where  $P_{lm}(\cos\theta)$  are the associated Legendre polynomials.

The angular variable of the transport equation is discretized by the discrete ordinates method:

$$\begin{aligned} & \Omega_a \cdot \nabla \psi^g(r, \Omega_a) + \Sigma_t^g(r) \psi^g(r, \Omega_a) \\ &= \sum_{g'=0}^G \sum_{l=0}^N \frac{2l+1}{4\pi} \Sigma_{sl}^{gg'}(r) [Y_{l0}^e(\Omega_a) \phi_{l0}^{g'}(r) \\ &+ \sum_{m=1}^l (Y_{lm}^e(\Omega_a) \phi_{lm}^{g'}(r) + Y_{lm}^o(\Omega_a) \vartheta_{lm}^{g'}(r))] + q_e^g(r, \Omega_a), \quad (7) \end{aligned}$$

where  $\Omega_a$  presents a given discrete direction.  $\psi^g(r, \Omega)$  are decomposed into two parts:

$$\psi^g(r, \Omega) = \psi_{(u)}^g(r, \Omega) + \psi_{(c)}^g(r, \Omega), \quad (8)$$

where  $\psi_{(u)}^g(r, \Omega)$  denotes the uncollided angular flux, and  $\psi_{(c)}^g(r, \Omega)$  denotes the collided flux. Equation (8) can be decomposed into the following two equations:

$$\Omega \cdot \nabla \psi_{(u)}^g(r, \Omega) + \Sigma_t^g(r) \psi_{(u)}^g(r, \Omega) = q_e^g(r, \Omega), \quad (9)$$

$$\begin{aligned} & \Omega \cdot \nabla \psi_{(c)}^g(r, \Omega) + \Sigma_t^g(r) \psi_{(c)}^g(r, \Omega) \\ &= \sum_{g'=0}^G \sum_{l=0}^N \frac{2l+1}{4\pi} \Sigma_{sl}^{gg'}(r) \sum_{m=-l}^l Y_{lm}(\Omega) \phi_{lm}^{g'(c)}(r) \\ &+ q_s^{(u)}(r, \Omega), \quad (10) \end{aligned}$$

$\psi_{(u)}^g(r, \Omega)$  can be calculated analytically

$$\psi_{(u)}^g(r, \Omega) = \delta(\Omega - \Omega_{p \rightarrow r}) \frac{q_0}{4\pi} \frac{e^{-\tau(r, r_p)}}{|r - r_p|^2}, \quad (11)$$

where  $r_p$  denotes the location of point source, denotes the location of targeting grid.  $\tau(r, r_p)$  is the optical distance between  $r$  and  $r_p$ .  $|r - r_p|$  is the distance between  $r$  and  $r_p$ .

The spherical harmonic moments of the uncollided angular flux become:

$$\phi_{lm}^{g(u)}(r) = Y_m(\Omega_{p \rightarrow r}) \frac{q_0}{4\pi} \frac{e^{-\tau(r,r_p)}}{|r-r_p|^2}, \quad (12)$$

$q_s^{(u)}(r, \Omega)$ , the first collision source, can be resolved using spherical harmonics.

$$q_s^{(u)}(r, \Omega) = \sum_{g'=0}^G \sum_{l=0}^N \frac{2l+1}{4\pi} \Sigma_{sl}^{gg'}(r) \sum_{m=-l}^l Y_{lm}(\Omega) \phi_{lm}^{g'(u)}(r). \quad (13)$$

First, RAY3D applies a ray-tracing technique to obtain the numerical values of distances and optical distances between all point sources and all targeting grids respectively. Then, we use Eq. (11) to obtain the uncollided angular flux. Equation (12) is then used to calculate the spherical harmonic moments of the uncollided flux. The calculation of the first collision source is accomplished by Eq. (13). The collided flux is calculated by the discrete ordinates method. The uncollided angular flux and collided flux make up the total flux.

### 3 Kobayashi benchmarks

In 1996, Kobayashi proposed [4] several 3D radiation transport benchmarks for simple geometries with a void region at OECD/NEA to examine the accuracy of codes. The benchmark problems consist of three regions [6]: the source, the void, and the shield regions, as shown in Fig.

1. Only Problem 2 is presented because the models of Problem 2 is similar to the CSNS target station neutron beamline shutter model.

The information of source strength and cross section [6] are presented in Table 1.

The numerical results of Monte Carlo code MCNP [7] and TORT3.2 [8] with FNSUNCL3 [9] for the 3D radiation transport benchmarks have been presented by Chikara Konno [10]. In Fig. 2, MCNP solutions are plotted as a reference and TORT solutions with FNSUNCL are plotted for comparison.

TORT and DONTRAN3D are both codes which employ the discrete ordinates method to solve the transport equation and obtain neutron or photon flux distribution. TORT is an authoritative discrete ordinates code developed by Oak Ridge National Laboratory. FNSUNCL is a corresponding ray effects elimination code for TORT, while RAY3D is the corresponding ray effects elimination code for DONTRAN3D.

Kobayashi's benchmarks were also calculated by DONTRAN3D and DONTRAN3D with RAY3D respectively. Fig. 2 plots the ratio of the calculated total neutron fluxes to those of the MCNP solutions.

The results of total neutron fluxes calculated by DONTRAN3D with RAY3D show good agreement with the MCNP solutions. For the cases with pure absorber, the maximum ratio is less than 4%. For the half scattering cases, the maximum ratio is less than 13%. This indicates that ARES is a reliable code system for shielding calculations.

Table 1. Information of source strength and cross section.

region	$S/(\text{n}\cdot\text{cm}^{-3}\cdot\text{s}^{-1})$	$\Sigma_t/\text{cm}^{-1}$	case i $\Sigma_s/\text{cm}^{-1}$	case ii $\Sigma_s/\text{cm}^{-1}$
1	1	0.1	0	0.05
2	0	$10^{-4}$	0	$0.5 \times 10^{-4}$
3	0	0.1	0	0.05

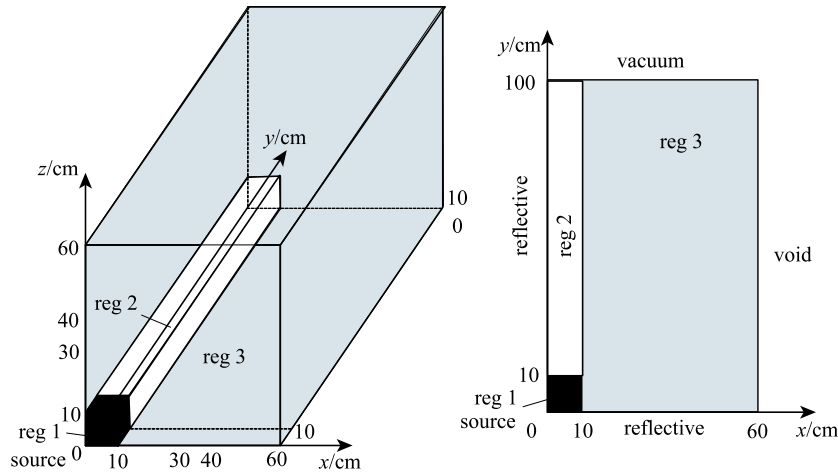


Fig. 1. Geometry of Problem 2.

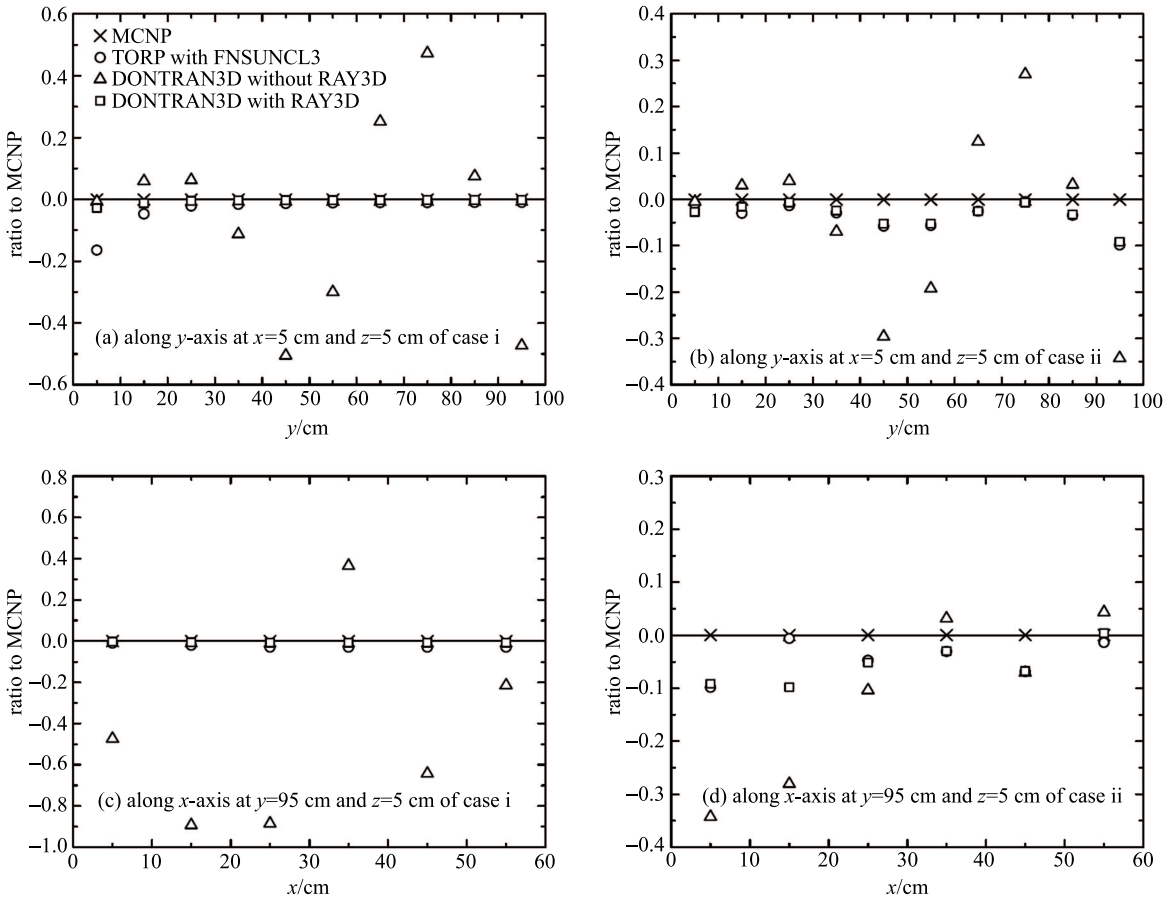


Fig. 2. Ratio of calculated total fluxes of prob. 2.

#### 4 CSNS target station neutron beamline shutter model and calculation parameters

The CSNS target station neutron beamline shutter model [11] is shown in Fig. 3. The height of the model is up to 10 m and the width of the model is 1.15 m.

The width of the void region is 11 cm and the void region is cut by stainless steel 316 at the height of 100 cm to 450 cm when the shutter is closed. Stainless steel 316 ranging from 100 cm to 250 cm contains a void region, as shown in Fig. 3(c), and the width of this void region is 5 cm. In Fig. 3(b), the width of stainless steel 316 ranging from 250 cm to 450 cm is 15 cm, and the material of the rest of the model is low carbon steel. The volume of the source region is 1 cm<sup>3</sup> and it is located at the bottom-left corner in Fig 3(d). In this CSNS target station neutron beamline shutter model, boundary surfaces ( $x=0$ ,  $y=0$  and  $z=0$ ) are treated as reflective boundary conditions. Other boundary surfaces are treated as void boundary conditions. Table 2 [11] lists the chemical compositions of stainless steel 316 and low carbon steel.

The model consists of 237276(39×39×156) rectan-

gular solids. There are high-energy neutrons in the CSNS target station, so a high-energy (up to 150 MeV)

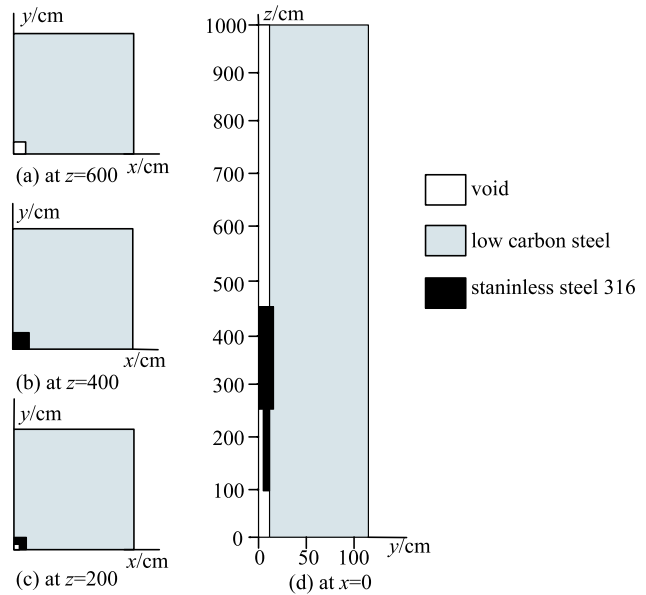


Fig. 3. The CSNS target station neutron beamline shutter model.

multi-group library set named HEST 1.0 [12] with 253 neutron and 48 photon groups is introduced. The library is developed based on ENDF/B-VII.0 [13] using the NJOY code [14]. We condense the 253 neutron group and 48 photon group into a 31 neutron group and 10 photon group respectively.  $P_3$ -order expansion in the Legendre polynomials of the scattering cross-section matrix is introduced, and  $S_8$  fully symmetrical quadrature sets, which approximate the flux angular discretization, are employed.

Table 2. The material chemical compositions.

material	density	chemical components/(wt.%)
stainless steel 316	8.03	iron (65.375%), chromium(17.0%), nickel(14.5%), manganese (2.0%), silicon(1.045%), carbon(0.08%)
low carbon steel	7.04	iron(99.1%), manganese(0.45%), silicon(0.25%), carbon(0.2%)

### 5 Results and analysis

To illustrate that the ray effects are a common problem of discrete ordinates codes and that they are unacceptable in the CSNS target station neutron beamline shutter problem, we present the distribution of dose rate at the height of 0 to 1000 cm ( $x=0$  cm,  $y=0$  cm) using TORT and DONTRAN3D respectively. We then calculate the same model using DONTRAN3D with RAY3D. The results of dose rate distribution at heights of 0 to 1000 cm ( $x=0$ ,  $y=0$ ) are shown in Fig. 4.

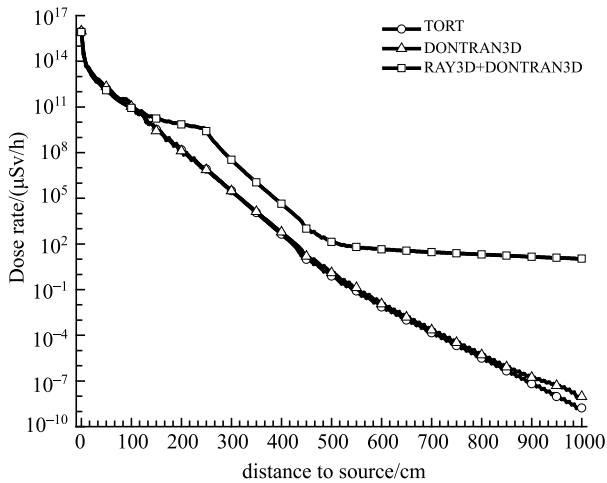


Fig. 4. The total dose axial distribution using TORT and DONTRAN.

As shown in Fig. 4, from  $z=0$  cm to  $z=450$  cm, the results obtained by TORT are nearly the same as the results calculated by DONTRAN3D. At heights of 450 cm to 1000 cm, which is a region without the strong shielding action of stainless steel 316, the results of TORT and

DONTRAN3D decline rapidly along the  $z$ -axis. The results of DONTRAN3D appear to be an order of magnitude greater than those of TORT at  $z=1000$  cm. The difference is caused by the different difference scheme. In DONTRAN3D, DZ (diamond set to zero difference scheme) is employed, while WD (weighted difference scheme) is employed in TORT. The unreasonable decline indicates that it is infeasible to solve the CSNS target station neutron beamline shutter problem just using discrete ordinates code. In this kind of problem with a void region and small source region, the ray effects are especially serious. As can be seen in Fig. 4, the results of DONTRAN3D with RAY3D are obviously different. At heights of 250 cm to 450 cm, the dose rate declines rapidly along the  $z$ -axis because of the shielding of stainless steel 316. The most obvious difference between the results of DONTRAN3D and DONTRAN3D with RAY3D appears at heights of 450 cm to 1000 cm. In this void region, the result of DONTRAN3D with RAY3D decreases much more smoothly along the  $z$ -axis. So, with the ray effect elimination effect of RAY3D, the results are more reasonable. The dose rate at  $z=1000$  cm is  $10.83 \mu\text{Sv/h}$ .

To intuitively show the comparison of results calculated by DONTRAN3D and DONTRAN3D with RAY3D, the distribution of fluxes in an arbitrary group is chosen to be presented. Figure 5 provides contour plots of the scalar flux of energy group 1. To show the distribution of all groups, Fig. 6 provides contour plots of the total dose rate using DONTRAN3D and DONTRAN3D with RAY3D.

In Fig. 5 and Fig. 6, darker color signifies larger flux. In the CSCS target station neutron beamline

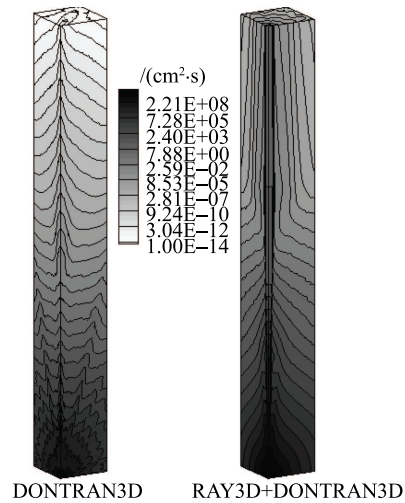


Fig. 5. Scalar flux distribution of energy group 1 along the  $y-z$  plane at  $x=0$ .

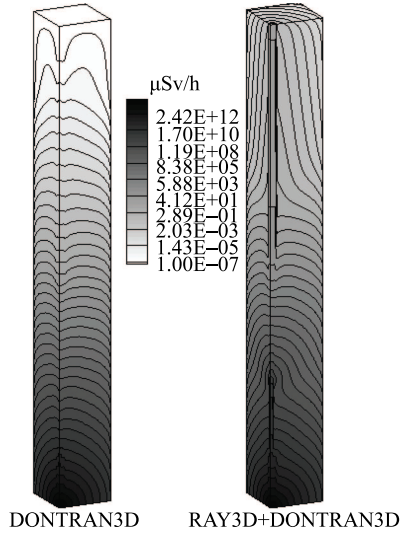


Fig. 6. Total rate dose distribution along the  $y$ - $z$  plane at  $x=0$ .

shutter model, even in the void region, the flux distribution shows rapid decline in all regions. This unreasonable phenomenon indicates that this kind of deep penetration problem with a channel of up to 10 m cannot be solved only by discrete ordinates code because of the strong ray effects. The distribution is obviously relatively reasonable after employing the first collision source method to attenuate the ray effects.

## 6 Radiation damage calculation

The possible damage induced by radiation in different solid materials has been a topic of great interest for engineering designers. In the CSNS target station, because of the large number of neutrons with high energy, radiation damage should be considered. The radiation damage mainly consists of atom displacement and gas generation. Displacement per atom (DPA) magnitude is commonly used to express atom displacements, which induce lattice dislocation and lattice imperfection. Therefore, atom displacements induce changes of properties in those materials. DPA can be used to predict the material changes induced by radiation. In this paper, only the radiation damage caused by neutrons is discussed.

The calculation procedure of DPA used in this work follows the idea implemented by the authors in [15]. DPA can be calculated by Eq. (14). DPA in a material gets higher over time.

$$\begin{aligned} \text{DPA} &= \left( \int \sigma_{\text{dpa}}(E) \cdot \phi(E) \cdot dE \right) \cdot t \\ &= \left( \sum_{g=1}^G \sigma_{\text{dpa},g} \phi_g \right) \cdot t \end{aligned} \quad (14)$$

where  $\sigma_{\text{dpa}}$  denotes the displacements cross section and  $t$  denotes time. In this paper, the DPA per year is calculated.  $\sigma_{\text{dpa}}$  can be calculated as follow:

$$\sigma_{\text{dpa}}(E) = \frac{\beta}{2E_d} \sigma_{\text{damage}}(E). \quad (15)$$

In Eq. (15),  $\sigma_{\text{damage}}$  denotes the damage energy cross section and  $E_d$  denotes the displacement energy.  $\beta$  denotes the atom displacement efficiency.

The damage energy cross section of stainless steel 316 and low carbon steel can be obtained from HEST1.0 [12]. The displacement energy of stainless steel 316 is 40 eV [15]. The displacement energy of low carbon steel is 40 eV, because its major component is iron, and the damage energy cross section of iron is 40 eV.

The DPA distribution in low carbon steel and stainless steel 316 are presented in Fig. 7 and Fig. 8 respectively.

The maximum DPA in low carbon steel region is 1.24 DPA/ $y$ , while the maximum DPA in stainless steel 316 region is 3.52E-03 DPA/ $y$ .

In the low carbon steel region, the DPA maximum (1.24 DPA per year) is located near the opening of the channel neutron beamline entrance. At this local area, material changes induced by radiation need special attention, because serious radiation damage may first appear in this area.

Nevertheless, the DPA in the whole stainless steel 316 region is low enough to be neglected.

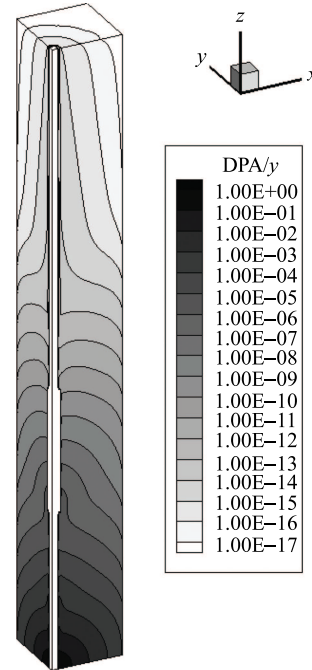


Fig. 7. DPA distribution in low carbon steel.

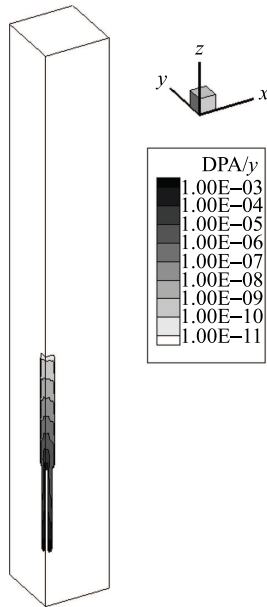


Fig. 8. DPA distribution in stainless steel 316.

## 7 Conclusions

RAY3D, which employs the first collision source method, can effectively mitigate the ray effects, and the ARES code system can effectively solve the CSNS target station neutron beamline shutter problem. The dose rate at the end of the neutron beam line is  $10.83 \mu\text{Sv/h}$ . Thus ARES provides an accurate tool for researchers to optimize a best engineering design in order to maintain a safe working environment and to minimize the cost of shielding materials.

There is still further work to do to make our code system perform better, like using the angle-integrated mesh-cell balance equation to modify the first collision source method [16], and developing a library with a higher upper limit of energy.

*The authors gratefully thank all members of CSNS Neutronics Group for their valuable work.*

## References

- 1 J. WEI, H. S. CHEN, Y. W. CHEN et al, Nucl. Instrum. Methods Phys. Res. A, **600**: 10 (2009)
- 2 Y. X. CHEN, B. ZHANG, Q. Y. ZANG et al, Energ. Sci. Tech., **47**(Suppl.): 477 (2013) (in Chinese)
- 3 T. A. Wareing, J. E. Morel, D. K. Parsons, A First Collision Source Method for ATTILA. In: *Proc. ANS RPSD Top. Conf.*, Nashville. (1998)
- 4 K. Kobayashi, OECD Proceedings, 403 (1997)
- 5 M. T. CHEN, B. ZHANG, Y. X. CHEN, Verification for Ray Effects Elimination Module of Radiation Shielding Code ARES by Kobayashi Benchmarks, In: *the 22nd Int. Conf. Nucl. Eng.*, Czech Republic, (2014)
- 6 K. Kobayashi, N. Sugimura, Y. Nagaya. *Prog. Nucl. Energ.*, **39**(2): 119 (2000)
- 7 J. F. Briesmeister, Los Alamos National Laboratory, 1997, Tech. Rep. LA-12625-M. (1997)
- 8 W. A. Rhoades, M. B. Emmett, Oak Ridge National Lab ,1982, Tech. Rep. ORNI/TM-8362, (1982)
- 9 K. Kosako, C. Konno, *Journal of Nucl. Sci. Tech.* , **37**(sup1): 475 (2000)
- 10 C. Konno, *Prog. Nucl. Energ.*, **39**(2): 167 (2001)
- 11 B. ZHANG, Y. X. CHEN, W. J. WU et al. *Chin. Phys. C.*, **35**(8): 791 (2011)
- 12 J. WU, Y. X. CHEN, W. J. WU et al. *Chin. Phys. C.*, **36**(3): 275 (2012)
- 13 M. B. Chadwick, P. Obložinský, M. Herman et al, *Nucl. Data sheets*, **107**(12), 2931 (2006)
- 14 R. E. MacFarlane, D. W. Muir, Los Alamos National Laboratory, 1994, Tech. Rep. LA-12740-M, (1994)
- 15 Q. Z. YU, W. Y. T. J. LIANG, *Acta Phys. Sin.*, **5**(5):194(2011) (in Chinese)
- 16 R. E. Alcouffe, R. D. O'Dell, Jr. F. W. Brinkley, *Nucl. Sci. Eng.*, **105**(2): 198 (1990)